Parametric analysis and multiobjective optimization for functionally graded foam-filled thin-wall tube under lateral impact

Article *in* Computational Materials Science · July 2014

DOI: 10.1016/j.commatsci.2014.03.044

CITATIONS
138

READS
462

5 authors, including:

Jianguang Fang
University of Technology Sydney
127 PUBLICATIONS **6,115** CITATIONS
SEE PROFILE

Yunkai Gao
Tongji University
58 PUBLICATIONS **2,019** CITATIONS
SEE PROFILE

Guangyong Sun
Hunan University
257 PUBLICATIONS **16,517** CITATIONS
SEE PROFILE

Qing Li
The University of Sydney
528 PUBLICATIONS **24,787** CITATIONS
SEE PROFILE

Computational Materials Science 90 (2014) 265–275

Contents lists available at ScienceDirect

Computational Materials Science

journal homepage: www.elsevier.com/locate/commatsci

Parametric analysis and multiobjective optimization for functionally graded foam-filled thin-wall tube under lateral impact

Jianguang Fang [a,c], Yunkai Gao [a,*], Guangyong Sun [b,*], Yuting Zhang [a], Qing Li [c]

[a] School of Automotive Studies, Tongji University, Shanghai 201804, China
[b] State Key Laboratory of Advanced Design and Manufacture for Vehicle Body, Hunan University, Changsha 410082, China
[c] School of Aerospace, Mechanical and Mechatronic Engineering, The University of Sydney, Sydney, NSW 2006, Australia

ARTICLE INFO

Article history:
Received 2 January 2014
Received in revised form 15 March 2014
Accepted 21 March 2014
Available online 5 May 2014

Keywords:
Functionally graded foam (FGF)
Three-point bending
Multiobjective optimization
Crashworthiness
Kriging model
Energy absorption

ABSTRACT

Foam-filled thin-walled tubes have proven an ideal energy absorber in automotive industry for its extraordinary energy-absorbing ability and lightweight potential. Unlike existing uniform foam (UF), this paper introduces functionally graded foam (FGF) to fill into the thin-walled structure subjected to lateral impact loading, where different configurations of foam grading (axial FGF and two transverse FGFs) are considered. To systematically investigate the bending behavior of this novel structure, numerical model is established using nonlinear finite element analysis code LS-DYNA and then is validated against the experiment. Through parametric study, it is found that the FGF tube absorbs more energy but may produce larger force than the UF counterpart. In addition, various parameters have a considerable effect on the crashworthiness performance of the FGF filled tube. Finally, multiobjective optimizations of UF and FGF filled columns are conducted, aiming to improve the specific energy absorption (SEA) and reduce the maximum impact force simultaneously, based upon the multiobjective particle optimization (MOPSO) algorithm and Kriging modeling technique. The optimization results show that all the FGF filled tubes can produce better Pareto solutions than the ordinary UF counterpart. Furthermore, the axial FGF tube provides better energy absorption characteristics than the two types of transverse FGF tubes.

1. Introduction

In vehicular systems, bumpers are expected to protect the driver and passengers when frontal crash occurs. The collision energy is absorbed by the bumpers subjected to bending condition. Likewise, side door beams or B-pillars are required to provide enough load-carrying capacity in the event of side impact. Therefore, it is of significance to investigate the bending behavior of thin-walled structures under lateral impact. Recently, cellular materials, especially metallic foams have aroused increasing attention for their extraordinary energy absorption capacity and lightweight potential in automotive industry. Inclusion of lightweight foam-fillers into thin-walled sections has proven an effective way to help increase the load-carry capacity and energy absorption. In this regard, several studies have been conducted on bending behavior of foam-filled thin-walled structures. For example, Santosa and Wierzbicki [1] explored the effect of ultralight metal fillers on the bending collapse behavior of thin-walled columns and pointed out that filling aluminum honeycomb or foam core is preferable to thickening the column wall in order to enhance the energy-absorbing efficiency. Chen [2] performed numerical simulations and experiments to study the crush behavior of thin-walled columns filled with aluminum foam and found the foam filler is capable of avoiding global failure thereby improving the load carrying capacity. Shahbeyk et al. [3] exploited the effect of various parameters, including spot welding failure, flange location, sheet metal thickness, glue presence and foam filling on the crash performance of empty and foam-filled box-beams. They concluded that aluminum foam filling can significantly change the bending behavior in terms of energy absorption and deformation patterns. Zarei and Kröger [4] applied crashworthiness optimization to maximize the specific energy absorption (*SEA*) of the squared empty and foam-filled columns with the constraint on the energy absorption and the results showed that the filled column can absorb the same energy as the optimal empty column but with a 28.1% lower weight. Guo and Yu [5] studied the dynamic response of foam-filled double cylindrical tubes under three-point bending experimentally and numerically. Compared to the traditional

* Corresponding authors. Tel./fax: +86 21 6958 9845 (Y. Gao). Tel.: +86 731 8881 1445; fax: +86 731 8882 2051 (G. Sun).
E-mail addresses: fangjg87@gmail.com (J. Fang), gaoyunkai@tongji.edu.cn (Y. Gao), sgy800@126.com (G. Sun).

http://dx.doi.org/10.1016/j.commatsci.2014.03.044
0927-0256/

foam-filled single tube, this new structure has a steadier load carrying capacity and much higher energy absorption efficiency under bending conditions. Besides, the maximum equivalent plastic strain of this structure increases much slower, which can provide a larger displacement to absorb more energy.

The above-mentioned studies are mainly restricted to uniform foam (UF) filled thin-walled structures. In order to further improve the crashworthiness of foam-filled structures, the functionally graded foam (FGF) material was recently used as an alternative to uniform foam (UF) material. Sun et al. [6] investigated the crash characteristics of FGF columns and first implemented the optimization procedure to seek optimum designs. Nouraei et al. [7] utilized nonlinear finite element code LS-DYNA to explore the crush behavior of FGF-filled columns under axial loading. Yin et al. [8] studied two kinds of functionally lateral graded foam-filled structures and the optimization was also performed to seek the optimal gradient exponential parameter. Most recently, based on dynamic ensemble metamodel, Yin et al. [9] conducted multiobjective crashworthiness optimization for a FGF filled tapered tube in order to simultaneously reduce the peak crushing force (*PCF*) and enhance the *SEA*. To the authors' best knowledge, however, previous studies on FGF-filled thin-walled structures did not take into account the bending behavior under lateral impact, which is a significant crashworthiness performance for thin-walled structures. Moreover, the effect of different grading directions (i.e., transverse and axial) on bending behavior was not investigated and compared in literature.

In this paper, the energy absorption characteristics of FGF filled tubes (including transverse and axial grading directions) under lateral impact loading are investigated by using nonlinear finite element code LS-DYNA. After the validation of finite element model, the effect of various parameters in the foam and wall on the crashworthiness performance is analyzed. Finally, multiobjective optimizations of UF filled tube and different types of FGF filled tubes are performed to simultaneously maximize the *SEA* and minimize the maximum impact force (F_{max}) by combining multiobjective particle optimization (MOPSO) algorithm with Kriging modeling technique.

2. Numerical modeling

2.1. Material modeling

The model selected to represent the material behavior of aluminum foam filler is Deshpande-Fleck foam (Material Model 154) which has been implemented as a user subroutine in LS-DYNA. The model was proposed by Deshpande and Fleck [10], in which the yield criterion of foam material is defined as follows:

$$\Phi = \hat{\sigma} - \sigma_y \leqslant 0 \tag{1}$$

where σ_y is the yield stress and the equivalent stress $\hat{\sigma}$ is given as:

$$\hat{\sigma}^2 = \frac{1}{[1+(\alpha/3)^2]}\left[\sigma_e^3 + \alpha^2\sigma_m^2\right] \tag{2}$$

where σ_e is the von Mises effective stress and σ_m the mean stress. Parameter α controlling the shape of the yield surface is a function of the plastic Poisson's ratio υ_p, given as:

$$\alpha^2 = \frac{9(1-2\upsilon_p)}{2(1+\upsilon_p)} \tag{3}$$

It is easily derived from Eq. (3) that $\alpha = 2.12$ when $\upsilon_p = 0$. The strain hardening rule is implemented in this material model as:

$$\sigma_y = \sigma_p + \gamma\frac{\hat{\varepsilon}}{\varepsilon_D} + \alpha_2 \ln\left[\frac{1}{1-(\hat{\varepsilon}/\varepsilon_D)^\beta}\right] \tag{4}$$

where $\hat{\varepsilon}$ is equivalent strain, σ_p, α_2, γ, β and ε_D are the material parameters and can be related to the foam density as

$$\begin{cases} \left(\sigma_p, \alpha_2, \gamma, \frac{1}{\beta}, E_p\right) = C_0 + C_1\left(\frac{\rho_f}{\rho_{f0}}\right)^\kappa \\ \varepsilon_D = -\ln\left(\frac{\rho_f}{\rho_{f0}}\right) \end{cases} \tag{5}$$

where ρ_f is the foam density and ρ_{f0} the density of base material. C_0, C_1 and κ are the constants as listed in Table 1. Note that the Young's modulus of foam material E_p is also a function of ρ_f as shown in Eq. (5) [11].

In this study, both axial and transverse FGF materials are considered, where the foam is discretized to several layers and in each layer the density is uniform. Fig. 1 depicts the grading pattern for the axial FGF, whose density changes along the axis and has symmetry about the mid-span plane of the beam. Fig. 2a and b displays the grading patterns for the transverse FGF, where the foam density changes along the height direction of the beam section and is symmetrical about the horizontal mid-plane, and along the two directions of the beam section respectively. The density gradient is determined by the following power-law functions:

$$\rho_f(x,m) = \begin{cases} \rho_{\min} + (\rho_{\max} - \rho_{\min})\left(\frac{x}{L}\right)^m & \text{for an ascending pattern} \\ \rho_{\max} - (\rho_{\max} - \rho_{\min})\left(\frac{x}{L}\right)^m & \text{for a descending pattern} \end{cases} \tag{6}$$

where $\rho_{\min}$ and $\rho_{\max}$ are the minimum and maximum densities, respectively. x and L represent the distances shown in Figs. 1 and 2. m denotes the gradient exponent parameter that governs the variation of foam density. Fig. 3a and b shows the variation of foam density along the grading direction for ascending and descending pattern respectively. In our case of bending tube to be explained in detail, the beam has a large bending deformation at the contact area with the punch (Fig. 4) whereas other parts undergo a rigid body rotation. Since the strong interaction between the tube wall and FGF has a positive influence on the energy absorption characteristics, the large stiffness of foam is expected at the large deformation area [7]. That is to say, the outermost layer should have the maximum density for transverse FGF and the middle section for the axial FGF in our specific case. Accordingly, the ascending pattern is selected for the axial FGF and the descending pattern for the two types of transverse FGF.

Regarding the material modeling of the tube wall, a bilinear elastic–plastic behavior with strain hardening (material model 24 in LS-DYNA) was adopted. The thin wall material was aluminum alloy AlMg0.5F22 with the following mechanical properties: density $\rho = 2700\ \text{kg/m}^3$, Poisson's ratio $\nu = 0.29$, Young's modulus $E = 68{,}566$ MPa, initial yielding stress $\sigma_y = 227$ MPa and tangential

Table 1
Material constants for aluminum foam [11,12].

Parameter	σ_p (MPa)	α_2 (MPa)	$1/\beta$	γ (MPa)	E_p (MPa)
C_0 (MPa)	0	0	0.22	0	0
C_1 (MPa)	720	140	320	42	0.33×10^6
κ	2.33	0.45	4.66	1.42	2.45

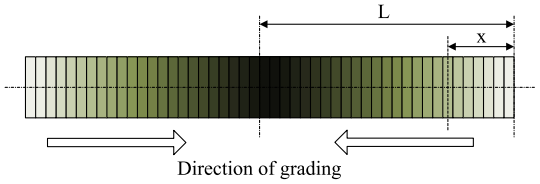

Fig. 1. Schematic showing grading patterns in axial direction.

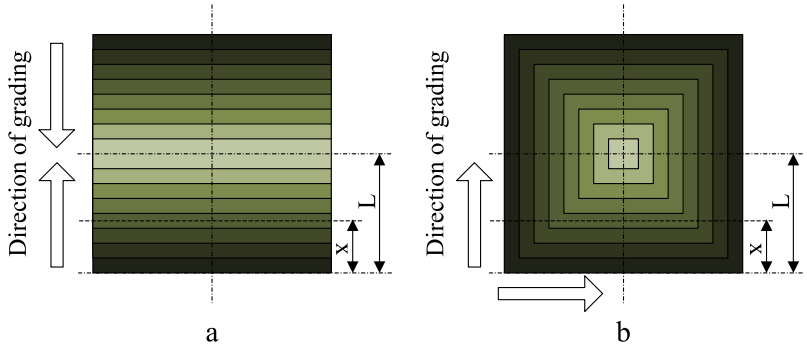

Fig. 2. Schematic showing two different grading patterns in transverse direction.

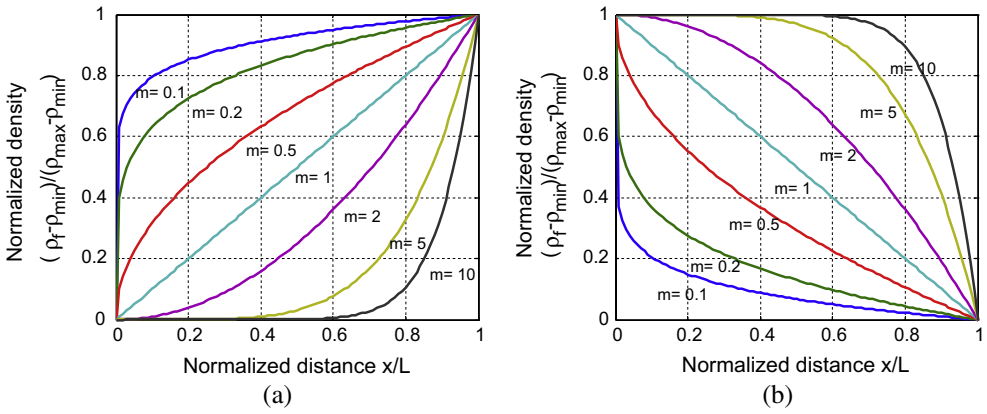

Fig. 3. Variation of foam density versus normalized distance: (a) ascending gradient pattern and (b) descending gradient pattern.

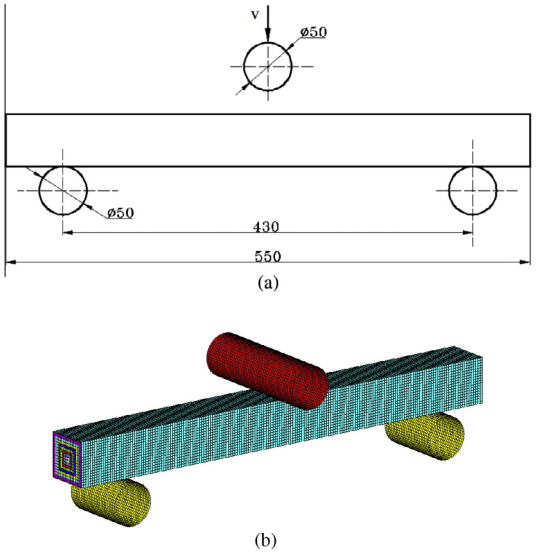

Fig. 4. Square beam with graded foam-filler: (a) schematic and (b) finite element model.

modulus of elasticity $E_t = 321$ MPa [13]. As the aluminum is insensitive to the strain rate, the rate-dependent effect is neglected in the FE modeling [14].

2.2. Finite element modeling

The structure analyzed herein is a functionally graded foam (FGF) filled thin-walled square tube subjected to lateral impact loading (Fig. 4). The length of beam is 550 mm, and the side length of the section is 55 mm. The foam-filled tube lays on two cylindrical supports, and the span and diameters are 430 mm and 50 mm respectively. A cylindrical punch with a diameter of 50 mm and a mass of 128 kg impacts onto the column at an initial velocity of $v = 4.4$ m/s in the mid-span.

The finite element models are developed using explicit nonlinear finite element code LS-DYNA. Fig. 4b shows the mesh used to model the bending of foam filled beam. The Belytschko-Lin-Tsay reduced integration shell elements with five integration points through the thickness were employed to model the tube walls. To model foam materials, solid elements with one integration point were adopted. The punch and supports were treated as rigid bodies. Stiffness-based hourglass control was employed to avoid spurious zero energy deformation modes and reduced integration was used to avoid volumetric locking.

Since the foam-filled tube involves two different materials, different contact algorithms in LS-DYNA can be used. The interface between the foam and wall was modeled as an "automatic surface to surface" contact. "Automatic single surface" contact was also prescribed to the tube wall and foam themselves to avoid interpenetration generated during bending. To account for contacts between the punch and beam, and between the supports and beam, "automatic surface to surface" contacts are defined with static and dynamic coefficients of friction of 0.2 and 0.3, respectively [15].

In order to decide the size of elements, a convergence test was carried out to minimize the effect of mesh refinement on the accuracy of the numerical results. It is found that the optimal mesh sizes for the tube and foam are 3×3 mm^2 and $3 \times 3 \times 3$ mm^3, respectively, which were able to converge within a reasonable computing time and were used throughout the study. In an ideal

functionally graded continuous model, the foam should be divided into an infinite number of layers. In the FE framework, the minimum depth of layer would be equal to the size of each solid element, which would however lead to very costly computational time. Furthermore, increasing the number of layers could increase the risk of numerical instability in the model resulting from the use of smaller element sizes. In this study, we chose 16 and 60 layers for transverse and axial FGFs, respectively, in which each layer was small enough.

2.3. Validation of the numerical model

To validate the simulation models, the empty column with the same dimension was first investigated under the same transverse loading condition. Figs. 5 and 6 display the comparison of crash behavior between the experiment [4] and the simulation, in terms of impact force versus punch displacement curve and deformation pattern respectively. It can be seen that the force versus displacement curve of simulation is able to capture the true bending behavior, and the deformation pattern of simulation also agrees with that of experiment. Furthermore, the simulation model of foam-filled column was also validated experimentally. From Eq. (6), it is obvious that the functionally graded foam (FGF) will become an uniform foam (UF) when the parameter m equals to 0. Thus, the validation of the developed finite element model of FGF filled tube can be verified against the experimental data of the UF filled tube. From Figs. 7 and 8, the simulation results agree fairly well with the corresponding experimental results [4]. As a result, the FE models are considered accurate and effective for the subsequent parametric analysis and design optimization.

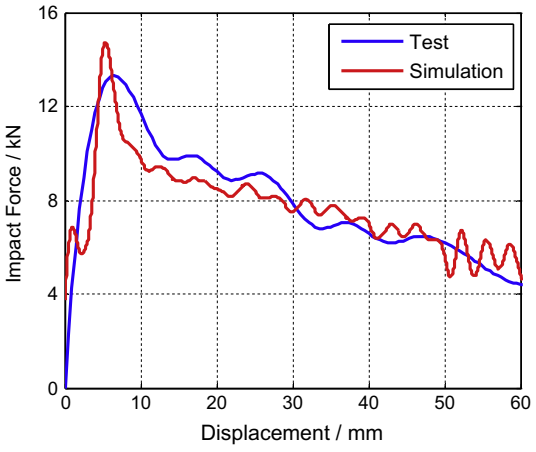

Fig. 5. Experimental [4] and numerical impact force curves for the empty beam.

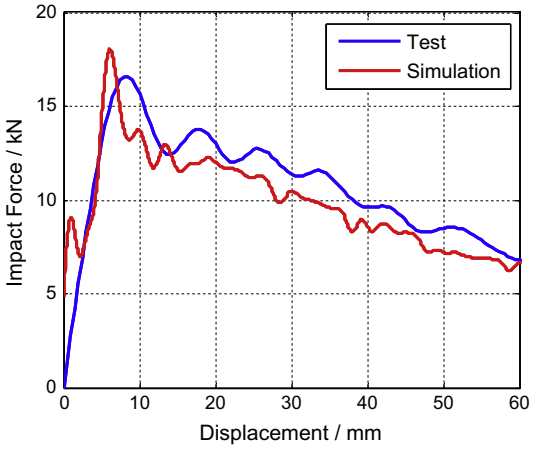

Fig. 7. Experimental [4] and numerical impact force curves for the foam-filled beam.

3. Parametric study

3.1. Crashworthiness criteria

To systematically study the crashworthiness of foam-filled thin-wall structures, it is essential to define the crashworthiness indicators. There have been many different indicators available to evaluate the crush characteristics and energy absorption capabilities of different structures [6,16]. Of these indicators, specific energy absorption (*SEA*) is widely used to estimate the energy absorption capabilities of structures with different materials and weights. *SEA* denotes the specific energy absorbed per unit mass of the absorber, as formulated below:

$$SEA = \frac{EA}{M} \tag{7}$$

where M is the total mass of foam-filler and thin-wall structure, and EA is the total absorbed energy during crashing, which can be calculated as:

$$EA = \int_0^{\delta} F(x)dx \tag{8}$$

where F is the impact force in axial direction and δ the crash displacement. Obviously, a higher *SEA* value indicates a higher capability of energy absorption.

Another indictor in relation to energy absorption capacity is crash load efficiency (*CFE*), which can be given as:

$$CFE = \frac{F_{avg}}{F_{\max}} \times 100\% \tag{9}$$

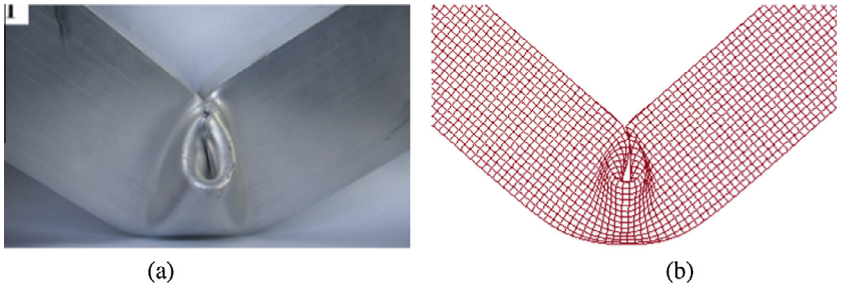

Fig. 6. (a) Experimental [4] and (b) numerical deformation patterns for the empty beam.

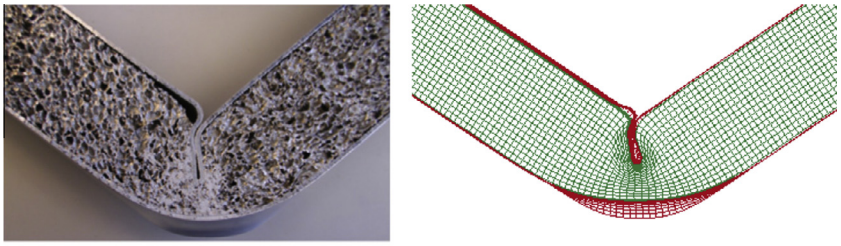

Fig. 8. (a) Experimental [4] and (b) numerical deformation patterns for the foam-filled beam.

where F_{max} is the maximum impact force when impact occurs, representing other critical indicator to the occupant survival rate as a large impact force often leads to a high deceleration and severe injury or even death of occupant. F_{avg} is the mean crash force, expressed as the total energy absorption divided by the corresponding crushing displacement,

$$F_{avg} = \frac{EA}{\delta} \tag{10}$$

In this study, the energy absorption (*EA*), specific energy absorption (*SEA*), crash force efficiency (*CFE*) and maximum force (F_{max}) are selected as the measurements of crashworthiness performance in subsequent parametric study and optimization.

3.2. Effect of density grading

In order to compare the energy absorption characteristics of UF and FGF filled tubes, numerical simulations were implemented based on the finite element models of the FGF beams with different values of gradient exponent parameter *m*. In each case, the other parameters were fixed: $\rho_{min} = 0.20\ g/cm^3$, $\rho_{max} = 0.50\ g/cm^3$, $\sigma_y = 227$ MPa and $t = 2.0$ mm (t denotes the wall thickness). Since the total mass of the FGF tube was varied, the UF tubes of the same weight as the corresponding FGF tubes were selected for comparing the crashworthiness. The equivalent foam density of UF tubes is calculated as follows,

$$\rho_{eqv} = \sum_{i=1}^{N_G} \rho_i / N_G \tag{11}$$

where N_G denotes the total number of layer of axial FGF, and ρ_i is the density of the ith layer.

Fig. 9a and b depicts the crashworthiness performance in terms of *EA* and *SEA* respectively. For all types of tubes, the larger the mass is, the more energy the tube absorbs. Furthermore, the FGF filled tubes, especially the axial FGF filled ones, can absorb more energy than the UF counterparts with the same mass. For the transverse FGF and UF filled beams, the *SEA* increases monotonically when the mass increases. On the other hand, for the axial FGF filled tubes, the *SEA* increases up to a peak value and then decreases with the increase of mass. Most importantly, the improvement of the FGF filled beams over the corresponding UF filled counterparts in *SEA* can be achieved. Considering the grading direction, the axial FGF filled beams seem more promising than the transverse FGF filled ones in terms of *EA* and *SEA*, which may be because that the axial grading concentrates the dense foam at the region of severe deformation (mid-span part of the beam) more efficiently.

Fig. 9c and d compares the F_{max} and *CFE* of the UF and FGF filled tubes, respectively. Generally, the axial FGF tubes have the highest values of F_{max} and *CFE* under the same mass while the UF tubes have the lowest values of F_{max} and *CFE*. While FGF beams can indeed produce larger *SEA* than the UF counterparts, they would lead to a larger F_{max}, which is also other key indicator to the safety of the occupants.

Note that all the crashworthiness criteria of UF and FGF beams converge to a same value when the mass increases. This is because that all the beams turn out to be a UF beam with the maximum foam density of $0.50\ g/cm^3$ when their masses increase up to the maximum value 0.67 kg.

To further explore the effect of the parameters of foam material and thin wall on the bending behavior of the FGF filled beam, we will conduct parametric analysis below by taking the axial FGF beam as an example belows.

3.3. Effect of density range

In order to explore the effect of foam density range ($\Delta\rho = \rho_{max} - \rho_{min}$) on the crashworthiness of FGF filled beams, the value of ρ_{min} was varied with 0.20, 0.25 and $0.30\ g/cm^3$ while the $\rho_{max} = 0.50\ g/cm^3$, $t = 2.0$ mm and $\sigma_y = 227$ MPa. Fig. 10a–d displays the *EA*, *SEA*, F_{max} and *CFE* of axial FGF filled beams at different values of grading exponent parameter *m*. Note that the density range ($\Delta\rho$) has a noticeable implication on crashworthiness performance. Specifically, large values of $\Delta\rho$ (small values of ρ_{min}) help improve *SEA*, although it could have a negative effect on *EA*. Besides, large values of $\Delta\rho$ could lead to small values of *CFE*, while it is able to reduce the values of F_{max}.

It should be noted that the crashworthiness performance is closely related to the value of *m*. When *m* increases for axial FGF filled beams with an ascending grading pattern, the intermediate foam density (between ρ_{min} and ρ_{max}) decreases (as shown in Fig. 3a), leading to the reduction of strengthening effect of the foam filler. As a result, the F_{max}, *CFE* and *EA* decrease monotonically with the increased *m*. On the other hand, the *SEA* first increases and then decreases with the increased *m* when the mass is taken into account.

3.4. Effect of wall thickness

In addition to foam material, the tube wall can also affect the crash behavior of the FGF filled beams. We varied the wall thickness with $t = 0.6$, 1.0, 1.5 and 2.0 mm while fixing other parameters (i.e., $\rho_{max} = 0.5\ g/cm^3$, $\rho_{min} = 0.2\ g/cm^3$, $\sigma_y = 227$ MPa), to quantify the effect on *EA*, *SEA*, F_{max} and *CFE*, and the results are shown in Fig. 11a–d. Interestingly, while thicker walls represent larger *EA* by the column, they do not produce larger *SEA*. Specifically, the *SEA* values with $t = 1.5$ mm are preferable, which are larger than those with a thicker wall ($t = 2.0$ mm) and thinner walls ($t = 1.0$ and 0.6 mm).

From Fig. 11c and d, it is found effective to reduce the F_{max} by thinning the wall directly. However, it is a more complicated relationship between the *CFE* and *t*, as the curve of $t = 0.6$ mm intersects with those of $t = 1.0$ and $t = 2.0$ mm.

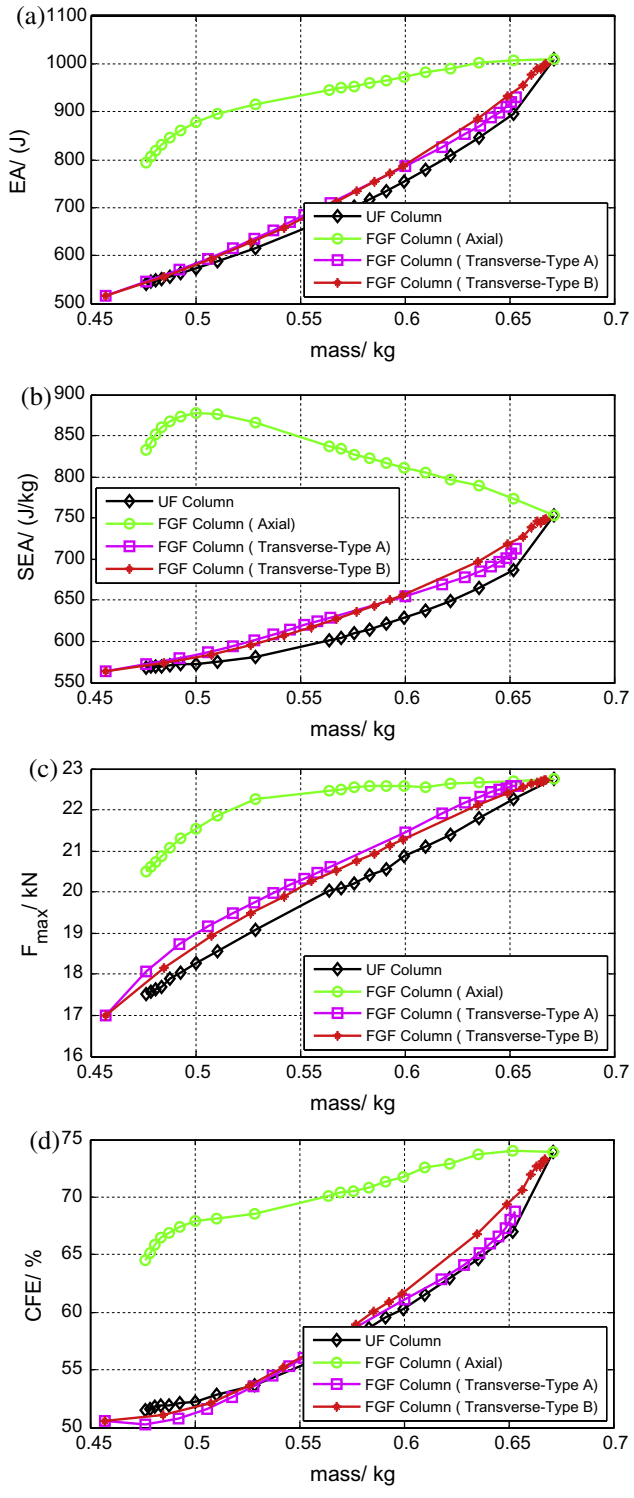

Fig. 9. Comparison of crashworthiness performance between UF and FGF filled beams: (a) *EA*, (b) *SEA*, (c) F_{max}, and (d) *CFE*.

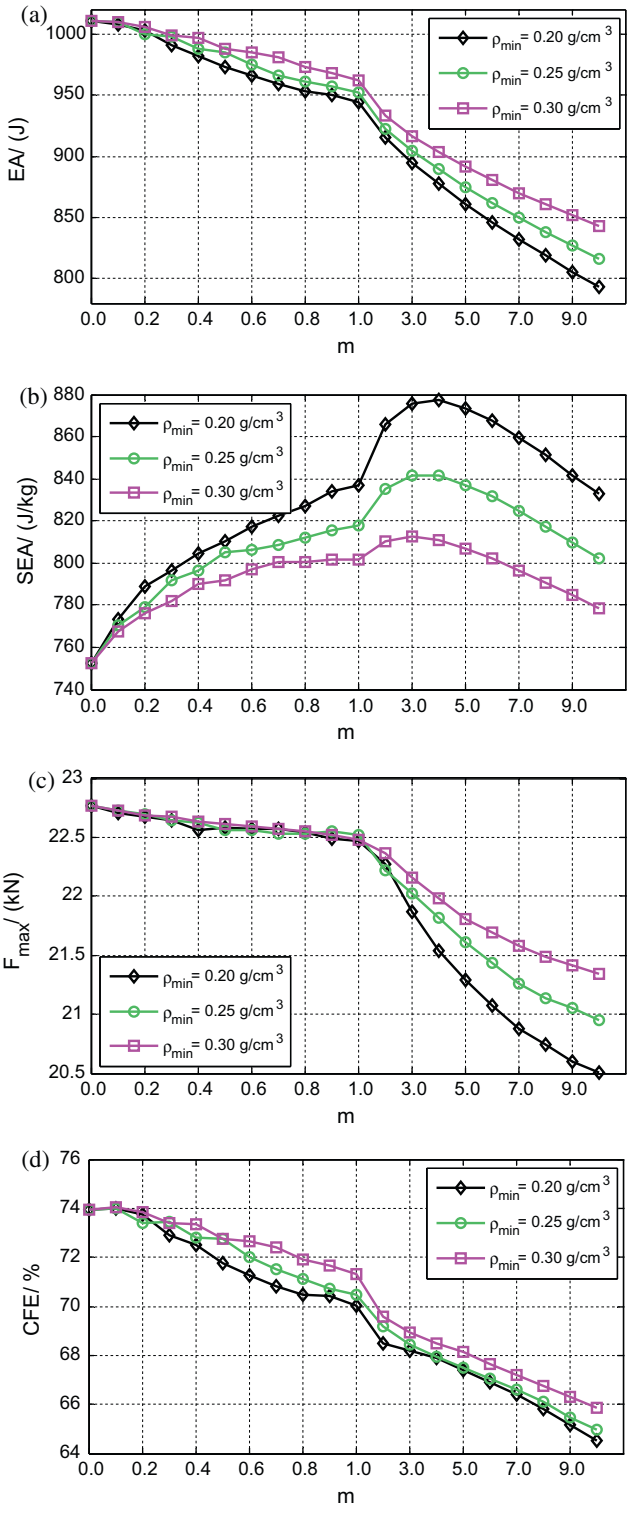

Fig. 10. Variation of crashworthiness performance due to density range: (a) *EA*, (b) *SEA*, (c) F_{max}, and (d) *CFE*.

3.5. Effect of wall yielding stress

The yielding stress was varied with $\sigma_y = 146$, 173, 200 and 227 MPa while $\rho_{max} = 0.5$ g/cm^3, $\rho_{min} = 0.2$ g/cm^3, $t = 2.0$ mm. Fig. 12a–d depicts the change of crashworthiness criteria due to the variation of σ_y. When $m \leqslant 4.0$, the axial FGF filled tubes with $\sigma_y = 200$ MPa can obtain the highest EA values. When $4 < m < 7$, the FGF columns $\sigma_y = 173$ MPa absorb the most energy in all the beams. When $m \geqslant 7$, the FGF tubes with $\sigma_y = 173$ and 227 MPa have the equal largest EA values. Since the variation of yielding stress does not change the tube mass at each specific case of m, the *SEA* values of different yielding stress follow the same order of magnitude as the EA values. The only difference is that the *SEA* values first increase and then decrease while the EA values decrease monotonically with the increased m.

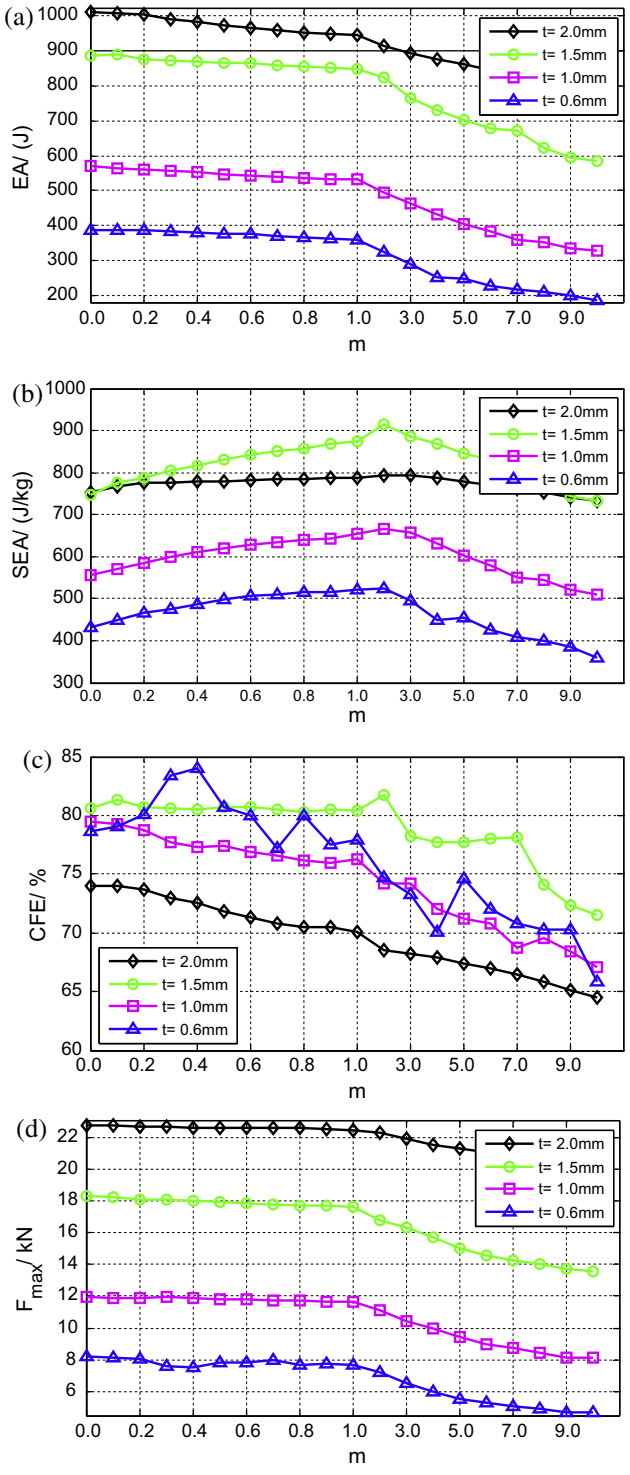

Fig. 11. Variation of crashworthiness performance due to wall thickness: (a) *EA*, (b) *SEA*, (c) F_{max}, and (d) *CFE*.

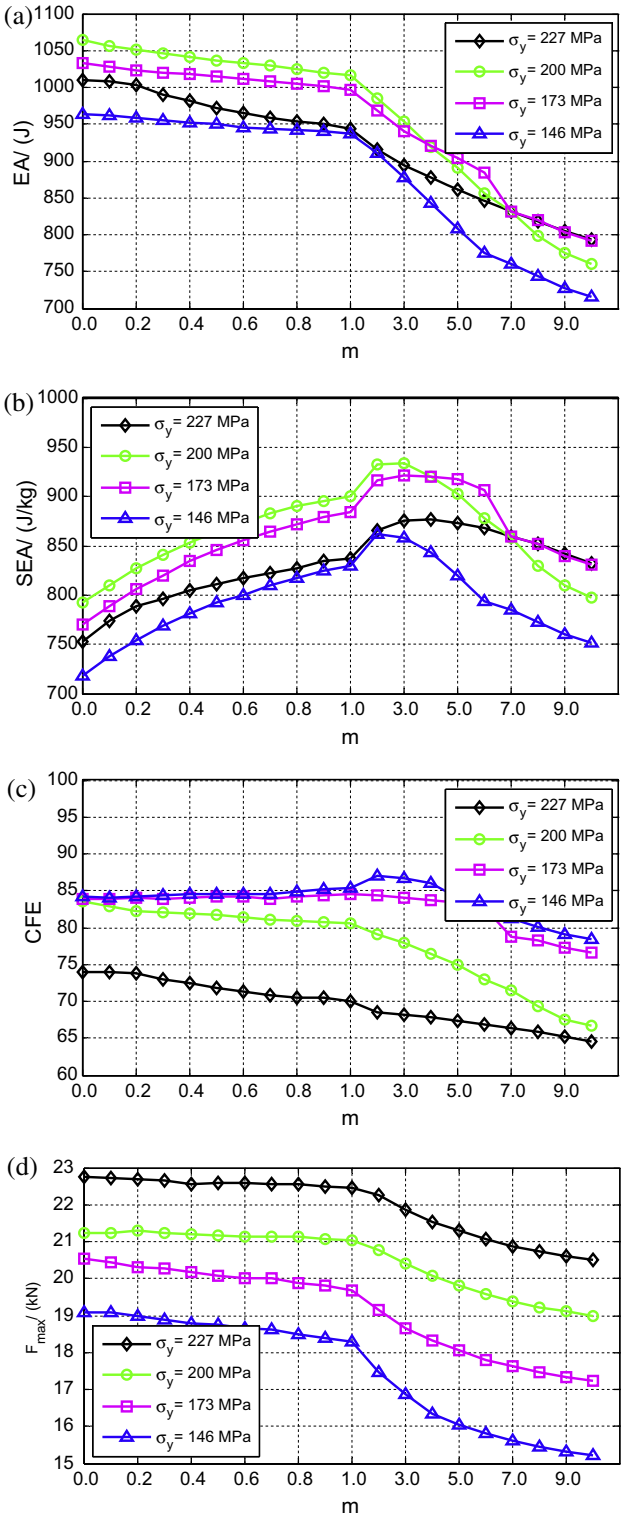

Fig. 12. Variation of crashworthiness performance due to wall thickness: (a) *EA*, (b) *SEA*, (c) F_{max}, and (d) *CFE*.

For F_{max} and *CFE*, the beams with $\sigma_y = 227$ MPa perform worst (i.e., have the largest F_{max} values and smallest *CFE* values) whilst the beams with $\sigma_y = 146$ MPa behave best (i.e., have the smallest F_{max} values and largest *CFE* values). Therefore, the tubes with low σ_y are preferred in terms of F_{max} and *CFE*. However, this conflicts with the requirements of *SEA* and *EA* by causing the smallest values of both *SEA* and *EA*.

To be brief, FGF filled beams perform better in *EA*, *SEA* and *CFE*, but worse in F_{max} than its UF counterparts. Besides, the parameters, including grading exponent m, density range ($\Delta\rho$), and wall thickness (t) and yielding stress (σ_y) could largely affect the crashworthiness of the FGF filled tubes.

3.6. Effect of the outermost layer density

As the outermost layer of transverse FGF directly contacts the wall, it is essential to investigate the effect of its density on

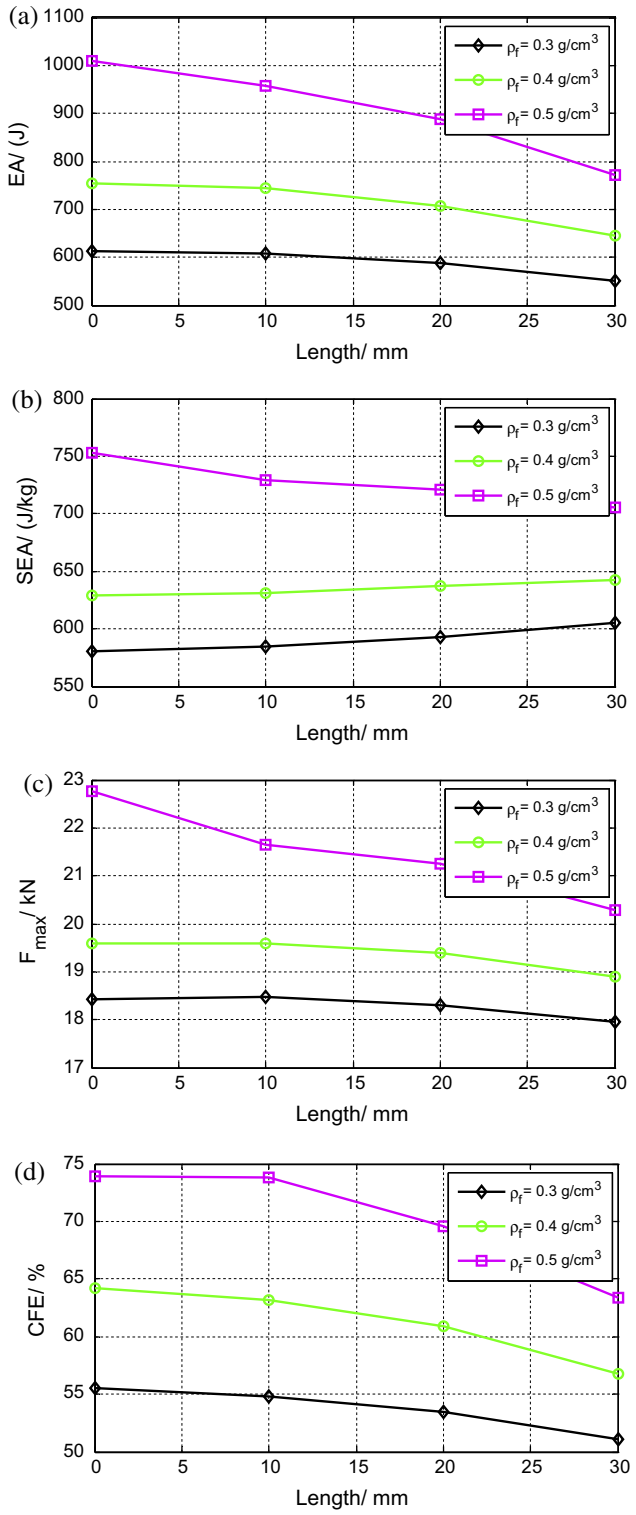

Fig. 13. Crashworthiness performance of the UF beams with different length of core removal: (a) *EA*, (b) *SEA*, (c) F_{max}, and (d) *CFE*.

crashworthiness. Numerical models based on three-point bending of the UF beam with $\rho_f = 0.3$, 0.4 and 0.5 g/cm^3 were established. The stiffness of the foam filler was reduced by removing the inner core and the removed cross sectional area were 0×0, 10×10, 20×20 and 30×30 mm^2. The *EA*, *SEA*, F_{max} and *CFE* for $\rho_f = 0.3$, 0.4 and 0.5 g/cm^3 with different core removal section lengths are plot in Fig. 13. When the removal length increases, the *SEA* of tube with $\rho_f = 0.5$ g/cm^3 decreases, but that of tube with $\rho_f = 0.3$ and 0.4 g/cm^3 increases, while the three other indicators in all cases reduce. Generally, the large foam density can absorb much energy and yield large crush force, meaning the dense foam helps strengthen the interaction between foam filler and thin wall.

4. Multiobjective optimization for functionally graded foam filled tubes

4.1. Optimization methodology

4.1.1. Definition of optimization problem

As an energy absorber, the beam structure is expected to absorb as much impact energy as possible per unit mass. Thus, the *SEA* should be an objective function and be maximized from the optimization perspective. Besides, the F_{max} of the structure is another important indicator for the safety of the occupants, which should be minimized.

While the effect of various parameters on crashworthiness behavior has been explored, it remains unknown how to design specific best designs for FGF filled thin-wall beam. Furthermore, the F_{max} fails to be reduced by using FGF filled beams, although the *SEA* is able to be increased from the parametric study. Therefore, we formulate the multiobjective optimization problems for the UF and FGF filled beams in Eqs. (12) and (13) respectively, aiming to simultaneously enhance these two design criteria. In the FGF problem the densities of foam can be varied by taking m as a design variable when $\rho_{max} = 0.5$ g/cm^3, $\rho_{min} = 0.2$ g/cm^3, while in the UF problem the density itself is taken as a design variable.

$$\begin{cases} \min & F_{max}, -SEA \\ s.t. & 0.6 \text{ mm} \leqslant t \leqslant 2.0 \text{ mm} \\ & 0.2 \text{ g/cm}^3 \leqslant \rho_f \leqslant 0.5 \text{ g/cm}^3 \\ & 140 \text{ MPa} \leqslant \sigma_y \leqslant 230 \text{ MPa} \end{cases} \tag{12}$$

$$\begin{cases} \min & F_{max}, -SEA \\ s.t. & 0.6 \text{ mm} \leqslant t \leqslant 2.0 \text{ mm} \\ & 0 \leqslant m \leqslant 10 \\ & 140 \text{ MPa} \leqslant \sigma_y \leqslant 230 \text{ MPa} \end{cases} \tag{13}$$

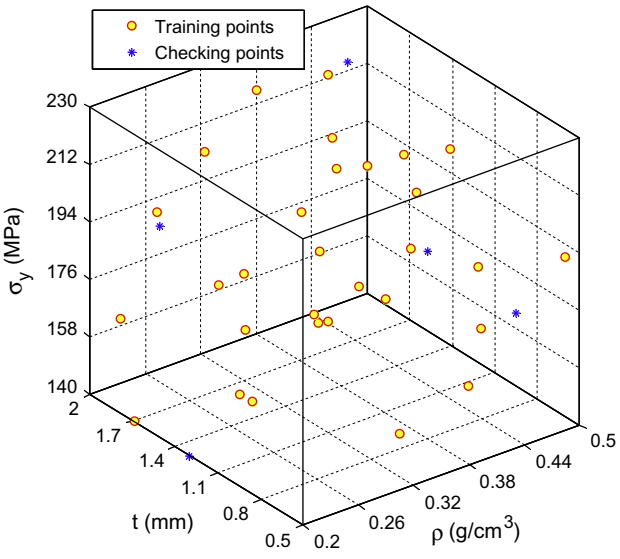

Fig. 14. Training points and checking points for the UF filled beam.

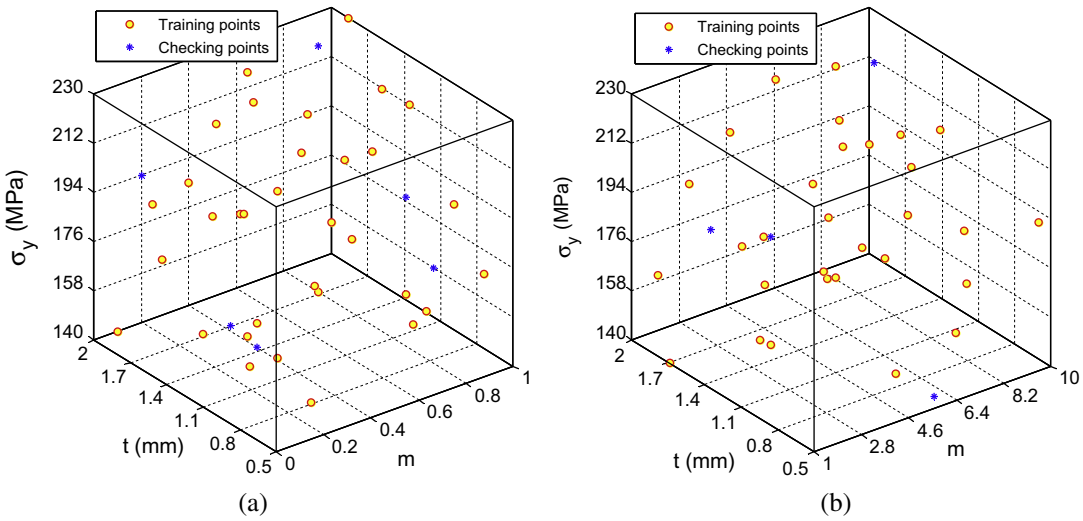

Fig. 15. Training points and checking points for the FGF filled beams: (a) $0 \leqslant m \leqslant 1$ and (b) $1 \leqslant m \leqslant 10$.

Table 2
Accuracy assessment of the Kriging models.

			R^2	e_{max}	e_{avg}
UF tube		F_{max}	0.9985	0.0271	0.0170
		SEA	0.9792	0.0476	0.0288
FGF tube (Axial)	$0 \leqslant m < 1$	F_{max}	0.9992	0.0298	0.0114
		SEA	0.9998	0.0086	0.0040
	$1 \leqslant m \leqslant 10$	F_{max}	0.9992	0.0189	0.0071
		SEA	0.9980	0.0252	0.0138
FGF tube (Transverse-Type A)	$0 \leqslant m < 1$	F_{max}	0.9996	0.0242	0.0087
		SEA	0.9520	0.0589	0.0267
	$1 \leqslant m \leqslant 10$	F_{max}	0.9890	0.0701	0.0394
		SEA	0.9866	0.0489	0.0209
FGF tube (Transverse-Type B)	$0 \leqslant m < 1$	F_{max}	0.9999	0.0077	0.0048
		SEA	0.9431	0.0604	0.0248
	$1 \leqslant m \leqslant 10$	F_{max}	0.9973	0.0266	0.0156
		SEA	0.9998	0.0046	0.0020

4.1.2. Surrogate model and error metrics

It is difficult to derive analytical objective functions mathematically for the *SEA* and F_{max} that involve highly nonlinear contact-impact and large deformation mechanics. As an alternative, surrogate modeling techniques, e.g. Kriging modeling, have proven rather effective and been widely implemented in crashworthiness design [17]. In practice, surrogate modeling techniques start with the sampling data at some training points. Design of experiment (DoE) is an approach to addressing how to select training points effectively. In this paper, the optimal Latin Hypercube sampling (OLHS) [18] is implemented to generate training points. Then the Kriging surrogate models are established to approximate the functions of *SEA* and F_{max}.

To assess the fitting accuracy of surrogate models, such metrics as *R*-square (R^2), maximum relative error (e_{max}) and average relative error (e_{avg}) are adopted as follows:

$$R^2 = 1 - \frac{\sum_{i=1}^{q}(y_i - \hat{y}_i)^2}{\sum_{i=1}^{q}(y_i - \bar{y})^2} \tag{14}$$

$$e_{max} = \max_{i\in\{1,\ldots,q\}}\left(\frac{|y_i - \hat{y}_i|}{|y_i|}\right) \tag{15}$$

$$e_{avg} = \frac{1}{q}\sum_{i=1}^{q}\frac{|y_i - \hat{y}_i|}{|y_i|} \tag{16}$$

where y_i denotes the exact function value for checking point i, $\hat{y}_i$ is the corresponding surrogate value. $\bar{y}$ is the mean of y_i, q is the number of the checking points. It can be seen that a larger value of R^2 is preferred, which indicates a higher accuracy for overall performance in the design space. On the other hand, smaller values of e_{max} and e_{avg} are preferred, which qualifies these relative errors at these checking points.

4.1.3. Multiobjective particle swarm optimization (MOPSO)

Particle swarm optimization (PSO) algorithm [19] is a relatively new heuristic algorithm inspired by the choreography of a bird flock. As an extended version of PSO, multiobjective particle swarm optimization (MOPSO) algorithm is characterized by fast convergence and well-distributed Pareto frontier compared with other multiobjective optimization algorithms such as NSGA-II [20,21], PEAS and microGA [22,23]. It is noted that MOPSO has been employed successfully to solve the design problems of sheet metal forming [24] and crashworthiness for FGF filled structures [6]. In this paper, the MOPSO proposed by Coello et al. [22] is utilized to handle the multiobjective optimization problems.

4.2. Results and discussion

4.2.1. Accuracy of Kriging models

Figs. 14, 15a and b display the training points and checking points over the design space for the UF beam, FGF beams with $0 \leqslant m \leqslant 1$ and FGF beams with $1 \leqslant m \leqslant 10$, respectively. Table 2 lists the results of accuracy assessment. It can be seen that the values of R^2 are all close to 1 and the values of e_{max} and e_{avg} are within 8%, indicating the Kriging models can be considered accurate adequately to replace the high-fidelity finite element analyses.

4.2.2. Results of multiobjective optimizations for the UF beam

Fig. 16 depicts the Pareto frontiers of different generations of the multiobjective optimization for the UF beam, where the settings of MOPSO are list in Table 3. Obviously, after 100 generations the Pareto frontier converges adequately. The Pareto optimal frontier provides designers with a set of solutions over the Pareto space for design selection. Specifically, if the designers pay more attention to *SEA*, the solutions at the top left corner should be selected. While if the designers emphasize on F_{max}, the solutions at the bottom right corner will be considered. To be compared with the optimized solution in the objective space, the initial design is also signified in Fig. 16. It can be seen that optimum A improves the

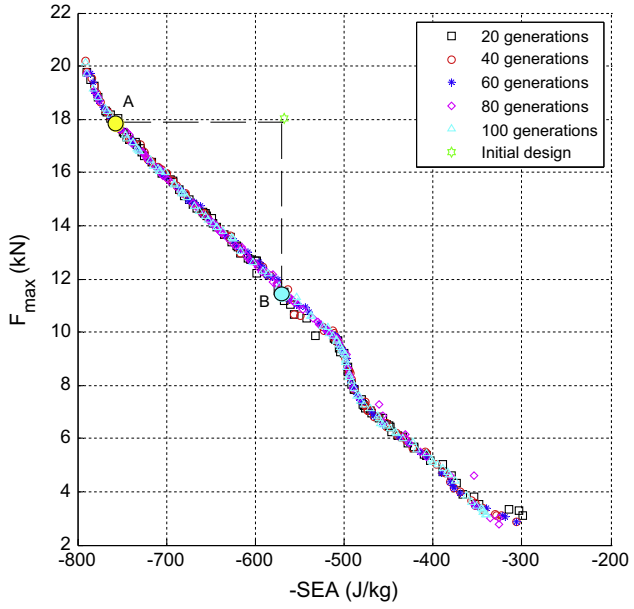

Fig. 16. Pareto frontiers of different generations for the UF filled column.

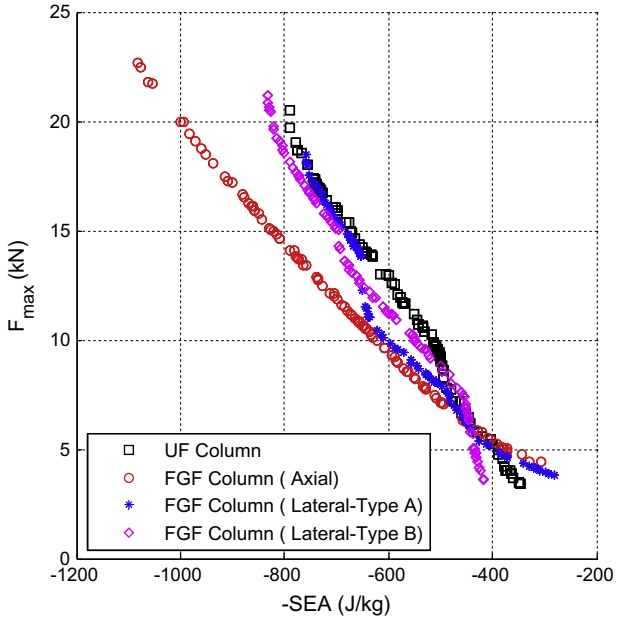

Fig. 17. Comparison of Pareto frontiers of UF filled column and FGF filled columns.

SEA when maintaining the F_{max}, whilst optimum B reduces the F_{max} when maintaining the *SEA*, in comparison to the initial design. The optimums between A and B can simultaneously reduce the F_{max} and increase the *SEA*.

4.2.3. Results of multiobjective optimizations for FGF beams

To compare the results of UF and FGF beams, their Pareto frontiers are plotted in Fig. 17 altogether. Similar to the Pareto frontier for the UF column, the Pareto frontiers of FGF filled beams present a series of solutions over the Pareto space, while parametric study just analyzes the effect of various parameters on crashworthiness performances and produces no specific optimal solution. Surprisingly, when UF is replaced with FGF, the Pareto frontiers move towards the direction representing the better performance in both *SEA* and F_{max}, except for those solutions at the bottom right corner. That is to say the FGF beams are able to increase the *SEA* and reduce the F_{max} simultaneously, which was not found in the previous parametric study.

Table 4 list the four optimal solutions for each tube, which are selected from the corresponding Pareto solutions subject to the constraint $F_{max} \leqslant 14$ kN. It can be seen that all the solutions have acceptable errors by comparing finite element analysis (FEA) results with Kriging values. The *SEA* values validated by FEA of the two types of transverse FGF filled beams are very close, indicating they have the equal effect on crashworthiness. Furthermore, optimization on the axial FGF beam produces the largest *SEA* value under the same level of F_{max}.

Note that partial foam filling in the vicinity of sever deformation can indeed reduce the foam mass while maintaining the load carrying capacity. However, foam-filled thin-walled tubes for potential applications could be subjected to more complicated loading. For example, in automotive engineering the bumper bar, front rail and firewall structures in frontal collision, the B-pillar in side collision and the A-pillar and roof frame structures in rollover accident could bend and deform at any local area. From the practical perspective, we decide to fill the whole tube rather than part of it.

Table 3
Settings of MOPSO.

MOPSO parameter name	Value
Population size	100
External archive size	100
Inertial weight	0.73
Personal learning coefficient	1.50
Global learning coefficient	1.50

Table 4
Optimal solutions (under the constraint of $F_{max} \leqslant 14$ kN).

	UF	Axial FGF	Transverse FGF	
			Type A	Type B
m (rho (kg/cm^3))	0.46	5.69	4.37	0.90
t (mm)	1.44	1.52	1.24	1.37
σ_y (Mpa)	166.55	199.34	225.70	219.33
F_{max} (kN)				
Kriging	13.99	13.84	13.86	14.00
FEA	13.79	13.80	14.13	14.54
Error	1.48%	0.32%	−1.89%	−3.75%
SEA (J/kg)				
Kriging	643.74	778.7	654.09	688.64
FEA	613.80	777.23	673.52	683.08
Error	4.88%	0.19%	−2.88%	0.81%

5. Conclusions

To explore the bending behavior of functionally graded foam (FGF) filled beams under lateral impact, the numerical model was established using non-liner finite element code LS-DYNA. The finite element model was then validated by the existing experiment data, in terms of impact force curve and deformation pattern. Through a parametric study, it was found that compared with the UF counterparts, the FGF beams would provide better values in the specific energy absorption (*SEA*), energy absorption (*EA*) and crash force efficiency (*CFE*), but worse values in the maximum impact force (F_{max}). The grading exponent parameter m of foam density, density range ($\Delta\rho$), wall thickness (t), yielding stress (σ_y) of wall material and the density of outermost layer could affect the crashworthiness performance significantly.

To further achieve the optimum design of crashworthiness for the UF and FGF filled beams, the multiobjective optimizations were formulated, aiming to simultaneously minimize the F_{max} and

maximize the *SEA*. The Kriging modeling technique and multiobjective particle optimization (MOPSO) algorithm were integrated to conduct the optimizations. The results show that the optimization of the FGF filled beams can yield better Pareto frontiers than the UF counterparts. Besides, the two transverse FGF filled tubes have the equal solutions, which are verified by finite element analysis (FEA). Furthermore, the optimum solutions from the axial FGF filled beams prove to be the most competent under the same constraints of F_{max}. To conclude, the novel structure of the FGF filled tube is worth studying and could be a potential energy absorber under lateral impact in engineering application.

Acknowledgements

The supports from The National 973 Project of China (2011CB711205), The National Natural Science Foundation of China (11202072), The Hunan Provincial Science Foundation of China (13JJ4036), The Doctoral Fund of Ministry of Education of China (20120161120005) for providing financial support. The first author is a recipient of the doctoral scholarships from both China Scholarship Council (CSC) and the University of Sydney.

References

[1] S. Santosa, T. Wierzbicki, Int. J. Mech. Sci. 41 (8) (1999) 995–1019.
[2] W. Chen, Int. J. Solids Struct. 38 (44–45) (2001) 7919–7944.
[3] S. Shahbeyk, A. Vafai, H.E. Estekanchi, Int. J. Crashworthiness 9 (6) (2004) 643–652.
[4] H.R. Zarei, M. Kröger, Int. J. Impact Eng 35 (6) (2008) 521–529.
[5] L. Guo, J. Yu, Int. J. Impact Eng 38 (2–3) (2011) 85–94.
[6] G. Sun, G. Li, S. Hou, S. Zhou, W. Li, Q. Li, Mater. Sci. Eng., A 527 (7–8) (2010) 1911–1919.
[7] M.S. Attia, S.A. Meguid, H. Nouraei, Finite Elem. Anal. Des. 61 (2012) 50–59.
[8] H. Yin, G. Wen, S. Hou, Q. Qing, Mater. Des. 44 (2013) 414–428.
[9] H. Yin, G. Wen, H. Fang, Q. Qing, X. Kong, J. Xiao, Z. Liu, Mater. Des. 55 (2014) 747–757.
[10] V.S. Deshpande, N.A. Fleck, J. Mech. Phys. Solids 48 (6–7) (2000) 1253–1283.
[11] A.G. Hanssen, O.S. Hopperstad, M. Langseth, H. Ilstad, Int. J. Mech. Sci. 44 (2) (2002) 359–406.
[12] A. Reyes, O.S. Hopperstad, T. Berstad, A.G. Hanssen, M. Langseth, Eur. J. Mech. A. Solids 22 (6) (2003) 815–835.
[13] J. Stropnik, F. Kosel, J. Therm. Stresses 34 (9) (2011) 893–910.
[14] S. Hou, Q. Li, S. Long, X. Yang, W. Li, Mater. Des. 30 (6) (2009) 2024–2032.
[15] M. Seitzberger, F.G. Rammerstorfer, H.P. Degischer, R. Gradinger, Acta Mech. 125 (1–4) (1997) 93–105.
[16] M.A. Guler, M.E. Cerit, B. Bayram, B. Gerceker, E. Karakaya, Int. J. Crashworthiness 15 (4) (2010) 377–390.
[17] Y. Gao, F. Sun, Int. J. Veh. Des. 57 (2011) 178–195.
[18] J. Fang, Y. Gao, G. Sun, Q. Li, Finite Elem. Anal. Des. 67 (2013) 13–21.
[19] R. Eberhart, J. Kennedy, in: Proceedings of the Sixth International Symposium on Micro Machine and Human Science, Nagoya Japan 1995, pp. 39–43.
[20] X. Liao, Q. Li, X. Yang, W. Zhang, W. Li, Struct. Multidiscip. Opt. 35 (6) (2008) 561–569.
[21] Y. Zhang, G. Sun, G. Li, Z. Luo, Q. Li, Mater. Des. 38 (2012) 99–109.
[22] C.A.C. Coello, G.T. Pulido, M.S. Lechuga, IEEE Trans. Evol. Comput. 8 (3) (2004) 256–279.
[23] C. Raquel, P. Naval, in: Proceedings of the 2005 Conference on Genetic and Evolutionary Computation, New York, NY, USA/Washington DC, USA, 2005, pp. 257–264.
[24] G. Sun, G. Li, Z. Gong, G. He, Q. Li, Eng. Opt. 43 (12) (2011) 1351–1366.